Physica D 51 (1991) 531–538
North-Holland

Decaying, two-dimensional, Navier–Stokes turbulence at very long times

W.H. Matthaeus[a], W.T. Stribling[a], D. Martinez[a], S. Oughton[a] and D. Montgomery[b]
[a]*Bartol Research Institute, University of Delaware, Newark, DE 19716, USA*
[b]*Department of Physics and Astronomy, Dartmouth College, Hanover, NH 03755, USA*

Two-dimensional Navier–Stokes turbulent decay has been followed numerically for very long times. The code is spectral, satisfies periodic boundary conditions, and does not make use of hyperviscosity or any small-scale smoothing. The resolution is $(512)^2$, the initial Reynolds number based on the box dimension is about 14000, and the run continues for over 290 initial eddy turnover times. Isolated vortices form, and the turbulence has become highly intermittent in the manner seen by McWilliams and Brachet et al., for times greater than about 30. However, it is *not* the case that merger of like-signed vortices stops; it only slows down. By $t = 210$, the final merger is complete, and the vorticity distribution is dominated by one large vortex of either sign. The negative (positive) vortices each occupy about two percent of the box area, and together account for over 98 percent of the total enstrophy. Their alignment suggests the formation of an Ewald lattice with a basic cell containing two point vortices. The ratio of enstrophy to energy continues to decrease monotonically, and the picture is consistent with a "selective decay" process, as described some time ago. A not-entirely-understood phenomenon is the concentration of the vorticity into two cores, suggestive of a negative-temperature state of the discrete line vortex model.

1. Introduction

The temporal decay of an initially turbulent two-dimensional Navier–Stokes flow has often been studied numerically, with a spatial resolution that has gradually increased with increasing computational capability (e.g. refs. [1–3]). It is known that the ratio of mean square vorticity ("enstrophy") to kinetic energy is a non-increasing function of time, and that the velocity field becomes increasingly dominated by the larger spatial scales as time progresses, since this ratio is essentially the square of the mean wavenumber that characterizes the spectrum. For high enough Reynolds numbers, the enstrophy can decay significantly while the energy is decaying by a negligible amount. About these assertions there has been no recent disagreement. This "selective decay" process [1, 4–12] and its generalizations have been proposed as explanations for relaxation phenomena in plasmas and in magnetofluids, for the case of decaying turbulence.

The dominant process by which the larger spatial scales assert themselves is the rather subtle one of like-sign vortex capture, which manifests itself visually on stream function and vorticity contour plots by showing increasingly larger and smoother structures as time progresses. The process is subtle because the smallest spatial scales are involved in the capture process, even though its net effect is the dominance of the energy spectrum by the largest scales.

In what were perhaps the most highly resolved two-dimensional (2D) Navier–Stokes computations at that time, McWilliams [2] carried out a detailed investigation of an evolving high-Reynolds number flow and noted a progressive decrease in the rate at which the vortex merger occurred. He hypothesized that it was possible that the merger process stopped or slowed down to a negligible rate, after which point isolated and non-interacting vortices drift about at large separations, with a cessation of spectral transfer.

In order to test this conjecture, we have repeated McWilliams' computation from initial conditions as close to his as possible. There are two principal differences between his computational situation and the one reported here: (1) we employ no hyperviscosity or small-scale smoothing of any kind; and (2) the temporal duration of the run is considerably longer (about 290 large-scale initial eddy turnover times). The spatial resolution is also slightly higher, here.

Over the time intervals computed by McWilliams, we find no disagreement with any of his conclusions. We find that over the longer time, however, all possible like-sign vortex captures occur, leaving us only with one vortex of either sign. The capture process has not ceased, but has only slowed down. The final-state stream function contours bear a striking resemblance to those for a basic cell of an Ewald lattice, a state to be expected from the Lin–Onsager discrete line–vortex model in the "negative temperature" regime [13–18].

An outline of this paper is as follows. In section 2, the essentials of the computation are outlined. In section 3, the computational results are summarized. Some discussion of the results follows in section 4.

2. Numerical procedures

We work in dimensionless units, inside a square box in the x, y plane, with edge length 2π; periodic boundary conditions are assumed. The fluid velocity $\boldsymbol{v} = \nabla \Psi \times \hat{\boldsymbol{e}}_z$, where the stream function $\Psi = \Psi(x, y, t)$ is independent of z, as are all other field variables. The vorticity $\boldsymbol{\omega} = \nabla \times \boldsymbol{v} = \omega \hat{\boldsymbol{e}}_z$, where $\omega = -\nabla^2 \Psi$. We work in the vorticity representation, in which we take the curl of the Navier–Stokes equation and solve

$$\frac{\partial \omega}{\partial t} + \boldsymbol{v} \cdot \nabla \omega = \nu \nabla^2 \omega. \qquad (1)$$

The kinematic viscosity ν can, in the dimensionless units, be interpreted as the reciprocal of a Reynolds number based on unit length and a unit initial rms velocity.

We use a fully dealiased Fourier Galerkin method of the Orszag–Patterson type [19–21]. The vorticity ω is expressed as the Fourier series $\omega = \sum_{\boldsymbol{k}} \omega(\boldsymbol{k}, t) \exp(i\boldsymbol{k} \cdot \boldsymbol{x})$, where the components of the $\boldsymbol{k}$'s are integers. The spatial resolution is $(512)^2$ with a maximum wavenumber of about 241, and a minimum of 1. All other fields are expressed as such Fourier series.

The modal energy is initialized according to the prescription $E(\boldsymbol{k}) \equiv \frac{1}{2}|\boldsymbol{v}(\boldsymbol{k})|^2 = C[1 + (\frac{1}{6}k)^4]^{-1}$ for $1 \le k \le 120$, and zero otherwise. We use a Gaussian random number generator, and choose random phases. This spectrum corresponds to an omni-directional energy spectrum that falls off as k^{-3} for large k. The positive constant C is chosen to give the initial kinetic energy per unit mass (defined as $E \equiv \sum_{\boldsymbol{k}} E(\boldsymbol{k}) = \frac{1}{2}\sum_{\boldsymbol{k}} k^{-2}|\omega(\boldsymbol{k})|^2$) the numerical value $\frac{1}{2}$. The enstrophy $\Omega \equiv \langle \frac{1}{2}\omega^2 \rangle = \frac{1}{2}\sum_{\boldsymbol{k}} |\omega(\boldsymbol{k})|^2$ has an initial value of about 67. (The brackets $\langle \ \rangle$ mean spatial averages.) The initial "palinstrophy" $P \equiv \frac{1}{2}\sum_{\boldsymbol{k}} k^2 |\omega(\boldsymbol{k})|^2$, which governs the enstrophy dissipation rate, is 1.61×10^5. This spectrum closely imitates the one used by McWilliams [2].

Several runs were carried out, and we shall report on the one with the highest Reynolds number and longest temporal duration: $R = \nu^{-1} = 14\,286$, extending to a time $t = t_{\max} = 292$. The time step is $\Delta t = (2048)^{-1}$. The initial large scale Reynolds number is much larger than an initial microscale Reynolds number based on an assumed enstrophy cascade: $R_l \equiv \Omega^{3/2}/2\nu P \cong 24.5$. The other, shorter runs exhibited behavior very similar to that which we report here.

3. Computational results

The computed ratio of enstrophy to energy, Ω/E, decays monotonically throughout the computation, as theory says that it must [11]. This is illustrated in fig. 1, in which we plot the mean square wave number $\sqrt{\Omega/E}$ versus time. The ratio reaches the final value 2.42 by $t = 292$, and is bounded from below by unity (when the only excited wavelength is the longest one allowed by the boundary conditions). Ω drops from about 67

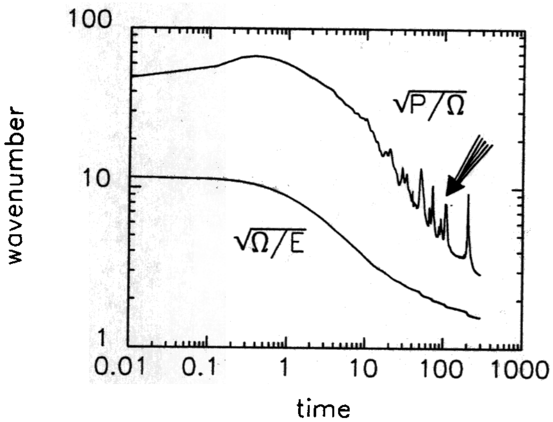

Fig. 1. Time history of the mean wavenumbers $\sqrt{\Omega/E}$ and $\sqrt{P/\Omega}$. Vortex captures at late times correspond to the sharp peaks in $\sqrt{P/\Omega}$; an arrow indicates the position of such a spike corresponding to a capture event discussed later in the text.

to about 1.0, while E is decaying only from 0.50 to about 0.41. Thus what is represented in fig. 1 is almost entirely the decay of enstrophy and it can only mean an increasing dominance of the spectrum by the longest wavelengths. Fig. 2 consists of three log–log plots of the angle-averaged modal spectra $E(k)$ and $\Omega(k)$ at early, intermediate and late times.

The dynamics are initially rather featureless and disordered as indicated by streamline plots (contours of constant Ψ) and vorticity contours both at $t = 1.0$, exhibited in figs. 3a and 3b. As time progresses the figures evolve greatly as shown in figs. 4a and 4b, which are contours of Ψ and ω, but now at $t = 292$.

A series of 3D perspective plots of surfaces of constant $\omega(x, y)$ versus x and y at six successive times constitutes figs. 5a–f. The gradual simplification of the topography occurs as a consequence of the recurrent like-signed vortex capture events, which are rather abrupt. For example, one occurs between figs. 5d and 5e. During this rather short time interval the smaller vortex indicated by the arrow is cannibalized by its near neighbor. Such captures followed closely have a rather detailed structure, not inconsistent in any way with the scenario proposed by Brachet et al. [3] for a very high-resolution study of vortex evolution. On a plot of $\sqrt{P/\Omega}$ (fig. 1), where P is the palinstrophy governing the enstrophy dissipation rate, the capture events of the kind that occur between figs. 5d and 5e have a gross manifestation of sharp spikes. These sudden enstrophy dissipation peaks on the $\sqrt{P/\Omega}$ curves can be correlated in a one-to-one fashion with the capture events of the kind that occur between figs. 5d and 5e.

The final state ($t = 292$) shows a concentration of about three fourths of the remaining single-sign vorticity and 98 percent of the enstrophy in two remaining maxima (minima). The separation and

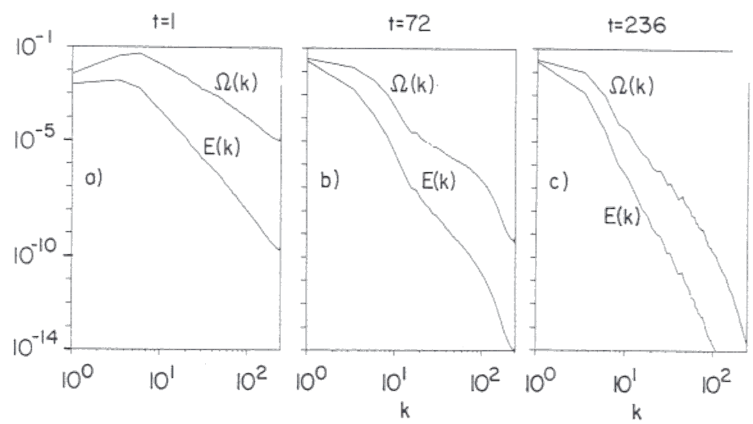

Fig. 2. Modal (direction averaged) spectra $E(k)$ and $\Omega(k)$ at (a) an early time ($t = 1$), (b) an intermediate time ($t = 72$) and (c) a late time ($t = 236$) in the run.

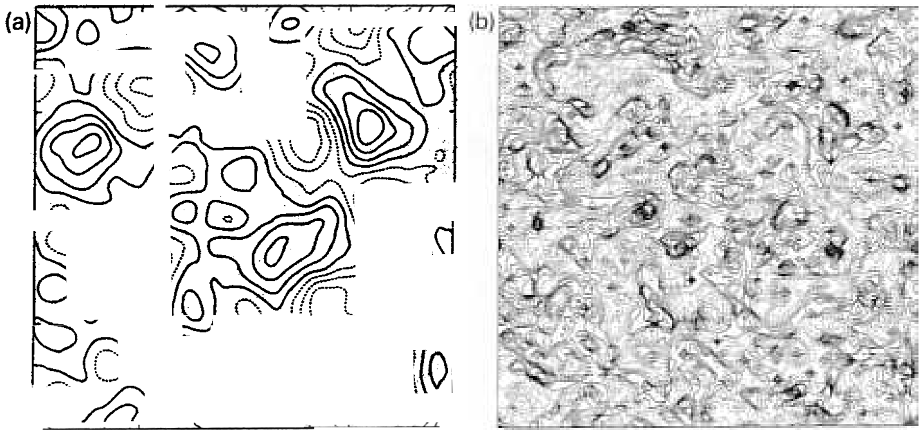

Fig. 3. (a) Stream function Ψ contours at $t = 1$, early in the run. (b) Vorticity ω contours at $t = 1$.

orientation of the peaks strongly suggest the locations of two oppositely signed vortices in their configuration of minimum interaction energy in the periodic box (maximum total energy, if the self-energy is included). This orientation is expected for the very high energy states of the ideal Lin–Onsager line–vortex system, which of course our continuous Navier–Stokes flow, with its nonsingular vorticity and enstrophy, is not. There is a not-altogether-understood emergence, at late times, of a particle-like character to the vorticity, and the states are similar to the "most probable states" predicted by the "sinh-Poisson" equation [15, 17, 18, 22] for line vortex systems. Fig. 6 illustrates the closeness of the late time simulation streamlines ($t = 292$, fig. 6a) to the streamlines associated with a two line vortex Ewald equilibrium (fig. 6b).

4. Discussion

In the evolution described in section 3, there are implications for some of the most central ideas in the theory of homogeneous turbulence: Kolmogorov similarity variables and their attendant power-law wavenumber spectra [23]. Underlying the dimensional analysis that leads to

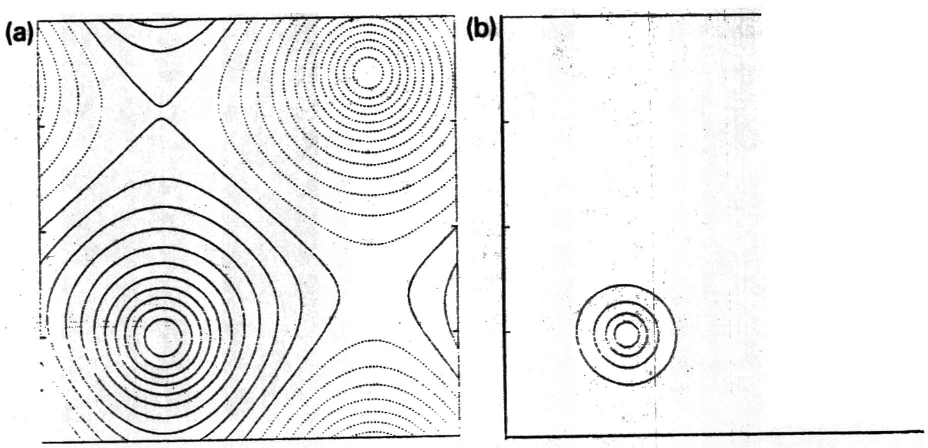

Fig. 4. (a) Stream function Ψ contours late in the run at $t = 292$. (b) Vorticity ω contours at $t = 292$.

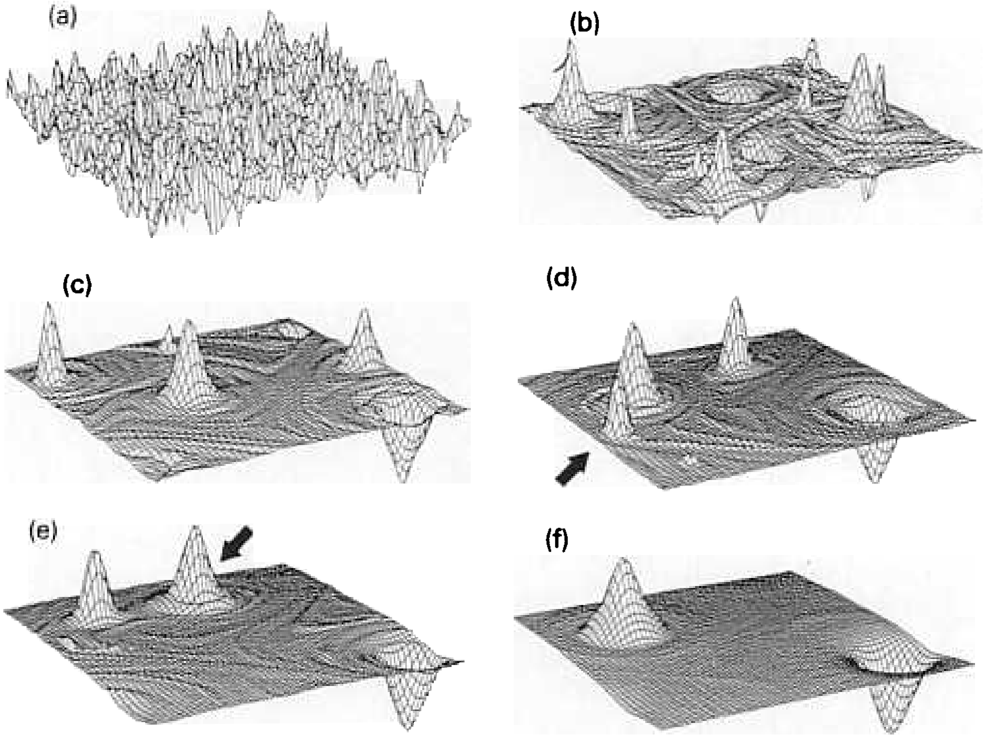

Fig. 5. 3D perspective plots of surfaces of constant $\omega(x, y)$ shown over the simulation domains at (a) $t = 1$, (b) $t = 28$, (c) $t = 58$, (d) $t = 94$, (e) $t = 118$ and (f) $t = 292$. In (d) arrows indicate positions of a smaller vortex and a larger one that undergo merger prior to $t = 118$. The position of the merged vortex is indicated by an arrow in (e).

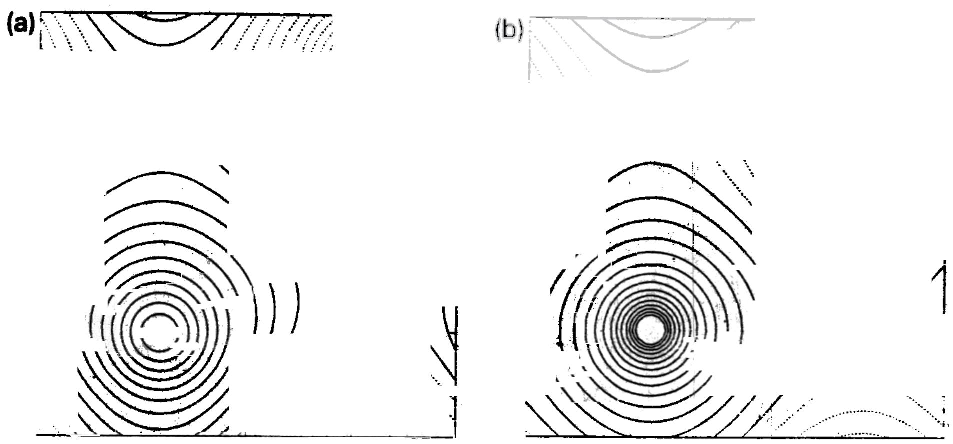

Fig. 6. (a) Streamlines from the decay run at a late time, $t = 292$. (b) Streamlines associated with a periodic equilibrium configuration of two equal strength oppositely signed line vortices.

inertial-range power law spectra is the idea that the energy spectrum contains the most important information, the phases are random, and different Fourier modes are uncorrelated. In any state such as the one illustrated in figs. 6a, 6b, phase relations among differing Fourier coefficients are clearly essential, and some of the most noteworthy features of the flow are not implied at all by the energy spectrum. Figs. 3a, 3b might comfortably fit in a Kolmogorov picture, but not figs. 4a, 4b or 6a. As also remarked recently by McWilliams, Kolmogorov-style cascade theories need to be reconsidered for flows dominated by coherent structures [24].

One useful lesson may be that the case of decaying "initial-value" turbulence is not the place to look for confirmation of power-law behavior and cascade spectra. The original Kolmogorov–Obukhov analysis [23] as well as the Kraichnan–Batchelor–Leith [25–27] generalization of it to two dimensions, assume a statistically steady injection rate for the cascaded quantities. It has sometimes been argued, at least for direct cascades to short wavelengths, that the steady injection-rate situation could be replaced by the effects of long-lived large eddies; confirmation or disproof of similarity-variable spectra have been sought within the framework of the pure initial-value problem.

The foregoing results cast doubt on the correctness of this procedure, suggesting that, the later the stages of 2D Navier–Stokes turbulent decay, the more likely the coherent vortices are to dominate the flow and interfere with the supposedly random and homogeneous cascade process. The development of coherent structures is by no means limited to the case of 2D Navier–Stokes flow, but also occurs in 2D and 3D magnetohydrodynamics, and possibly in 3D Navier–Stokes flow, though the detailed nature of the structures is different from case to case. The sometimes frustrating results of searches for "universal" power-law spectra (such as has been carried out, for example, in the solar wind) may seem a little less puzzling in this light. It may be that the departures from the predicted inertial-range power laws measure, among other things, how far advanced the evolution of a coherent-structure-dominated flow has become, and less-than-previously-expected degrees of "universality" may come to seem unsurprising.

As an example of the differences to be expected between the initial-value problem and the case of steady random injection, we close by displaying two previously unpublished figures for the driven case from the Ph.D. dissertation of Hossain [28]. (Several features of this computation, which dealt with the results from the driven

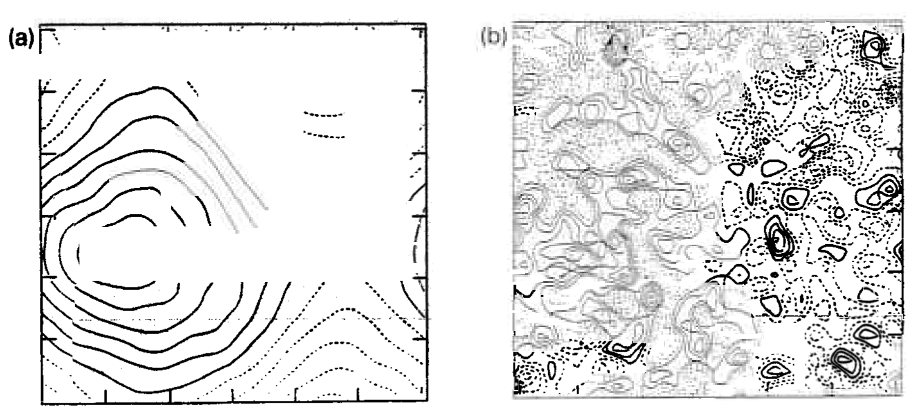

Fig. 7. (a) Streamlines late in a randomly driven run. (b) Vorticity contours from the same run at the same time. Taken from the Ph.D. thesis of Hossain [27, 28].

case at very long times, have already been published elsewhere [29].) In figs. 7a, 7b we show two contour plots showing curves of constant Ψ and ω for the randomly injected flow at late times ($t = 273$ characteristic times [29]). The streamlines (fig. 7a) from the driven run are quite similar to the streamlines in the present decay run at long times (e.g. fig. 6a). However the vorticity plots in the driven run (fig. 7b) and the decay run (fig. 6b) clearly have differences that apparently persist for arbitrarily long times. In particular, although the vorticity in the driven run is roughly segregated into clumps of positive and negative signed vorticity, there is no indication of the kind of sharply defined coherent vortex structure seen in the decay run.

As a final observation, which we do not wish to discuss here, we note that the evolution that has occurred in this computation has come close to a state of *minimum energy dissipation rate*, subject to the constraint implied by the remaining value of the total energy [12].

Note added in proof

A plot (not shown) of the integrated correlation coefficient of ω and $\sinh(\beta\psi)$ continues to increase as a function of time, and eventually reaches the value 0.97 by $t = 374$ for $\beta = -2.1$. (A correlation coefficient of unity would indicate a perfect "sinh-Poisson" solution [15].) This value is significantly larger than the correlation coefficient for ψ and ω directly.

Acknowledgements

This research has been supported in part by National Science Foundation Grant ATM-89131627 and NASA Grant NGT-50338 at Bartol, and NASA Grant NAG-W-710 and US Department of Energy Grants DE-FG02-85ER-53194 and DE-FG02-85ER-53298 at Dartmouth. The computations were supported by the National Science Foundation San Diego Supercomputing Center. We thank M. Hossain for providing us with figs. 7a and 7b.

References

[1] W.H. Matthaeus and D. Montgomery, Selective decay hypothesis at high mechanical and magnetic Reynolds numbers, in: Proc. Int. Conf. on Nonlinear Dynamics (1979), Ann. NY Acad. Sci. 357 (1980) 203.

[2] J.C. McWilliams, The emergence of isolated vortices in turbulent flow, J. Fluid Mech. 146 (1984) 21.

[3] M. Brachet, M. Meneguzzi, H. Politano and P.-L. Sulem, The dynamics of freely decaying two-dimensional turbulence, J. Fluid Mech. 194 (1988) 333.

[4] D. Montgomery, L. Turner and G. Vahala, Three-dimensional MHD turbulence in cylindrical geometry, Phys. Fluids 21 (1978) 757.

[5] S. Riyopoulos, A. Bondeson and D. Montgomery, Relaxation toward states of minimum energy in a compact torus, Phys. Fluids 25 (1982) 107.

[6] W.H. Matthaeus and D. Montgomery, Dynamic alignment and selective decay in MHD, in: Statistical Physics and Chaos in Fusion Plasmas, eds. W.H. Horton and L.E. Reichl (Wiley, New York, 1984) p. 285.

[7] J.P. Dahlburg, D. Montgomery, G.D. Doolen and L. Turner, Turbulent relaxation to a force-free field-reversed state, Phys. Rev. Lett. 57 (1986) 428.

[8] J.P. Dahlburg, D. Montgomery, G.D. Doolen and L. Turner, Turbulent relaxation of a confined magnetofluid to a force-free state, J. Plasma Phys. 40 (1988) 39.

[9] G.F. Carnevale and G.K. Vallis, Pseudo-advective relaxation to stable states of inviscid two-dimensional fluids, J. Fluid Mech. 213 (1990) 549.

[10] A. Hasegawa, Self-organization process in continuous media, Adv. Phys. 34 (1985) 1.

[11] A.C. Ting, W.H. Matthaeus and D. Montgomery, Turbulent relaxation processes in magnetohydrodynamics, Phys. Fluids 29 (1986) 3261.

[12] D. Montgomery and L. Phillips, MHD turbulence: relaxation processes and variational principles, Physica D 37 (1989) 215.

[13] C.C. Lin, On the motion of vortices in two dimensions (Univ. of Toronto Press, Toronto, 1943).

[14] L. Onsager, Statistical Hydrodynamics, Nuovo Cimento Suppl. 6 (1949) 279.

[15] G. Joyce and D. Montgomery, Negative temperature states for the two-dimensional guiding-centre plasma, J. Plasma Phys. 10 (1973) 107.

[16] T.S. Lundgren and Y.B. Pointin, Statistical mechanics of two-dimensional vortices, J. Stat. Phys. 17 (1977) 323.

[17] D.L. Book, B.E. McDonald and S. Fisher, Steady-state distributions of interacting discrete vortices, Phys. Rev. Lett. 34 (1975) 4.

[18] A.C. Ting, H.H. Chen and Y.C. Lee, Exact solutions of a nonlinear boundary value problem: the vortices of the two-dimensional sinh-Poisson equation, Physica D 26 (1987) 37.

[19] S.A. Orszag, Numerical simulation of incompressible flows within simple boundaries I. Galerkin (spectral) representations, Stud. Appl. Math. 50 (1971) 293.

[20] G.S. Patterson and S.A. Orszag, Spectral calculations of isotropic turbulence: Efficient removal of aliasing interactions, Phys. Fluids 14 (1971) 2358.

[21] C. Canuto, M.Y. Hussaini, A. Quarteroni and T.A. Zang, Spectral Methods in Fluid Dynamics (Springer, New York, 1987).

[22] C.E. Seyler Jr., Thermodynamics of two-dimensional plasmas or discrete line vortex fluids, Phys. Fluids 19 (1976) 1336.

[23] G.K. Batchelor, Theory of Homogeneous Turbulence (Cambridge Univ. Press, Cambridge, 1959).

[24] J.C. McWilliams, A demonstration of the suppression of turbulent cascades by coherent vortices in two dimensional turbulence, Phys. Fluids 2 A (1990) 547.

[25] R.H. Kraichnan, Inertial ranges in two-dimensional turbulence, Phys. Fluids 10 (1967) 1417.

[26] G.K. Batchelor, Computation of the energy spectrum in homogeneous two-dimensional turbulence, Phys. Fluids 12 (1969) II-233.

[27] C.E. Leith, Diffusion approximation for two-dimensional turbulence, Phys. Fluids 11 (1968) 671.

[28] M. Hossain, Long-time states of inverse cascades in the presence of a maximum length scale, Ph.D. Dissertation, College of William and Mary, Williamsburg, Virginia (1983).

[29] M. Hossain, W.H. Matthaeus and D. Montgomery, Long-time states of inverse cascades in the presence of a maximum length scale, J. Plasma Phys. 30 (1983) 479.